Inorg. Chem. **2005**, *44*, 2472–2482

Electrochemically Informed Synthesis and Characterization of Salts of the $[Pt_2(\mu\text{-}\kappa As,\kappa C\text{-}C_6H_3\text{-}5\text{-}Me\text{-}2\text{-}AsPh_2)_4]^+$ Lantern Complex Containing a Pt–Pt Bond of Order $^1/_2$

Martin A. Bennett,[†,‡] Suresh K. Bhargava,*[,†] John F. Boas,[§] René T. Boeré,[∥] Alan M. Bond,*[,⊥] Alison J. Edwards,[‡] Si-Xuan Guo,[⊥] Anton Hammerl,[#] John R. Pilbrow,[§] Steven H. Privér,[†] and Peter Schwerdtfeger[○]

School of Applied Sciences (Applied Chemistry), RMIT University, GPO Box 2476V, Melbourne, Victoria 3001, Australia, Research School of Chemistry, Australian National University, Canberra, A.C.T. 0200, Australia, School of Physics and Materials Engineering, Building 27, and School of Chemistry, Building 23, Monash University, Clayton, Victoria 3800, Australia, Department of Chemistry and Biochemistry, The University of Lethbridge, Lethbridge, AB T1K 3M4 Canada, Department of Chemistry, The University of Auckland, Private Bag 92019, Auckland, New Zealand, and Theoretical Chemistry, Building 44, Institute of Fundamental Sciences, Massey University at Albany, Private Bag 102 904, North Shore Mail Center, Auckland, New Zealand

Received September 23, 2004

Detailed electrochemical studies in dichloromethane (0.1 M Bu_4NPF_6) on the oxidation of the half-lantern $[Pt_2(\kappa^2 As,C\text{-}C_6H_3\text{-}5\text{-}Me\text{-}2\text{-}AsPh_2)_2(\mu\text{-}\kappa As,\kappa C\text{-}C_6H_3\text{-}5\text{-}Me\text{-}2\text{-}AsPh_2)_2]$ (**1**) and full-lantern $[Pt_2(\mu\text{-}\kappa As,\kappa C\text{-}C_6H_3\text{-}5\text{-}Me\text{-}2\text{-}AsPh_2)_4]$ (**2**) complexes reveal the presence of an exceptionally stable dinuclear Pt cation $\mathbf{2}^+$. Thus, oxidation of **1** occurs on the voltammetric time scale via a ladder-square scheme to give $\mathbf{2}^+$, whereas **2** is directly converted to $\mathbf{2}^+$. Electrochemically informed chemical synthesis enabled the isolation of solid $[\mathbf{2}^+][BF_4^-]$ to be achieved. Single-crystal X-ray structural analysis showed that $\mathbf{2}^+$ also has a lantern structure but with a shorter separation between the Pt centers [2.7069(3) Å ($\mathbf{2}^+$), 2.8955(4) Å (**2**)]. EPR spectra of $\mathbf{2}^+$ provide unequivocal evidence for axial symmetry of the complex and are noteworthy because of an exceptionally large, nearly isotropic hyperfine coupling constant of about 0.1 cm^{-1}. Spectroscopic data support the conclusion that the unpaired electron in the $\mathbf{2}^+$ cation is distributed equally between the two Pt nuclei and imply that oxidation of **2** to $\mathbf{2}^+$ leads to the establishment of the metal-to-metal hemibond. Results of extended Hückel molecular orbital and density functional calculations on **2** and $\mathbf{2}^+$ lead to the conclusions that s, p, d_{z^2} mixing of orbitals contributes to the large EPR Pt hyperfine coupling and also that the structural adjustments that occur upon removal of an electron from **2** are driven by the metal–metal bonding character present in $\mathbf{2}^+$.

Introduction

Reaction of 2-Li-4-$MeC_6H_3AsPh_2$ with $[PtCl_2(SEt_2)_2]$ gives two structurally characterized isomeric dinuclear platinum(II) complexes.[1] One isomer contains two chelating and two bridging $[C_6H_3\text{-}5\text{-}Me\text{-}2\text{-}AsPh_2]^-$ ligands in a half-lantern structure, $[Pt_2(\kappa^2 As,C\text{-}C_6H_3\text{-}5\text{-}Me\text{-}2\text{-}AsPh_2)_2(\mu\text{-}\kappa As,\kappa C\text{-}C_6H_3\text{-}5\text{-}Me\text{-}2\text{-}AsPh_2)_2]$ (**1**, Chart 1), and the other contains four bridging $[C_6H_3\text{-}5\text{-}Me\text{-}2\text{-}AsPh_2]^-$ ligands in a full-lantern structure, $[Pt_2(\mu\text{-}\kappa As,\kappa C\text{-}C_6H_3\text{-}5\text{-}Me\text{-}2\text{-}AsPh_2)_4]$ (**2**, Chart 1).

Halogens (X_2) react with **1** and **2** to give the same diplatinum(III) species $[Pt_2X_2(\mu\text{-}\kappa As,\kappa C\text{-}C_6H_3\text{-}5\text{-}Me\text{-}2\text{-}AsPh_2)_4]$ (**3**, Chart 1).[1] Attempts to prepare mixed-valent Pt(II)−Pt(III) complexes of the type $[Pt_2X(\mu\text{-}\kappa As,\kappa C\text{-}C_6H_3\text{-}5\text{-}Me\text{-}2\text{-}AsPh_2)_4]$ by comproportionation of **2** and **3** were unsuccessful, although analogous species, which in the solid state contain halide ligands connecting dinuclear lantern units,

* To whom correspondence should be addressed. E-mail: suresh.bhargava@rmit.edu.au (S.K.B.), alan.bond@sci.monash.edu.au (A.M.B.).
† RMIT University.
‡ Australian National University.
§ School of Physics and Materials Engineering, Building 27, Monash University.
∥ The University of Lethbridge.
⊥ School of Chemistry, Building 23, Monash University.
The University of Auckland.
○ Massey University at Albany.

(1) Bennett, M. A.; Bhargava, S. K.; Bond, A. M.; Edwards, A. J.; Guo, S.-X.; Privér, S. H.; Rae, A. D.; Willis, A. C. *Inorg. Chem.* **2004**, *43*, 7752.

10.1021/ic048660i CCC: $30.25
Published on Web 03/09/2005

Chart 1

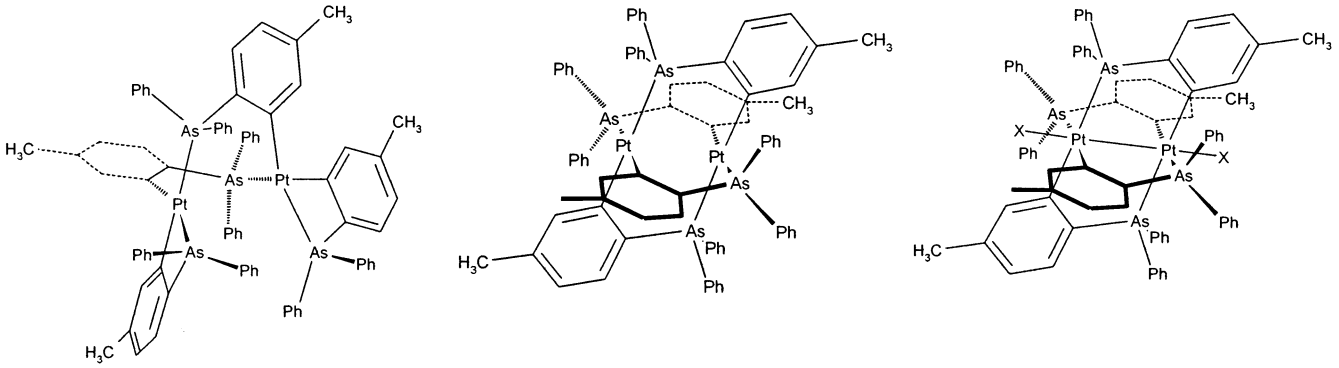

1 **2** **3**

are well-known in the corresponding μ-pop (pop = pyrophosphite, $P_2O_5H_2^{2-}$) and μ-dithioacetate series.[2] Here, we report detailed electrochemical and spectroelectrochemical studies of the oxidation of **2** that have led to the informed chemical synthesis and structural characterization of a rare form of, halide-free Pt(II)−Pt(III) cation, $[Pt_2(\mu\text{-}\kappa As,\kappa C\text{-}C_6H_3\text{-}5\text{-}Me\text{-}2\text{-}AsPh_2)_4]^+$, $\mathbf{2}^+$.

Experimental Section

General Comments. Dichloromethane (AnalaR grade) was obtained from BDH and dried over basic alumina. Nitrosonium hexafluorophosphate (Aldrich), ferrocene (Aldrich), and silver tetrafluoroborate (Pennwalt/Ozark-Mahoning) were used as received. Complexes **1** and **2** were synthesized as described in the literature.[1] Tetrabutylammonium hexafluorophosphate (Bu_4NPF_6) from GFS was purified as described in the literature.[3] Ferrocenium tetrafluoroborate[4] ($FcBF_4$) and ferrocenium hexafluorophosphate[5] ($FcPF_6$) were prepared by literature methods.

Elemental analyses were performed by the Microanalytical Unit at the Research School of Chemistry, Australian National University (ANU), Canberra, Australia, on samples dried at 40 °C in vacuo to remove residual solvent. Mass spectral data were obtained on a Bruker Biflex II MALDI-TOF spectrometer.

Chemical Synthesis of $\mathbf{2}^+$. To a yellow solution of complex **2** (102 mg, 0.061 mmol) in CH_2Cl_2 (20 mL) was added a blue suspension of $FcBF_4$ (17 mg, 0.062 mmol) in CH_2Cl_2 (10 mL). The solution immediately turned brown and then deep red/purple. After the mixture had been stirred for 10 min, the volume was reduced to ~5 mL. Ether (20 mL) was then added, causing a brown solid to precipitate that was filtered off and dissolved in CH_2Cl_2 (5 mL). Ether (20 mL) was again added, and the brown solid that reprecipitated was isolated, washed with ether, and dried in vacuo, giving 77 mg (72%) of $[\mathbf{2}^+][BF_4^-]$. MALDI-MS (*m*/*z*): 1667 $[M - BF_4]^+$. Anal. Calcd for $C_{76}H_{64}As_4BF_4Pt_2$: C 52.04, H 3.68. Found: C 51.60, H 3.80. The same salt can be prepared using $AgBF_4$ as the oxidant. In an analogous reaction, a solution of **2** (175 mg, 0.105 mmol) in CH_2Cl_2 (40 mL) was treated with a suspension of $FcPF_6$ (35 mg, 0.106 mmol) in CH_2Cl_2 (10 mL) to give a deep red/purple solution. Workup as above gave 160 mg (84%) of $[\mathbf{2}^+][PF_6^-]$. MALDI-MS (*m*/*z*): 1667 $[M - PF_6]^+$; Anal. Calcd for $C_{76}H_{64}As_4F_6PPt_2$: C 50.37, H 3.56. Found: C 50.12, H 3.49.

Attempts to grow single crystals of the PF_6^- salt by layering a CH_2Cl_2 solution of $[\mathbf{2}^+][PF_6^-]$ with ether resulted in significant decomposition, but a crystal selected from the resulting solid proved, surprisingly, to be the BF_4^- salt. The X-ray data were inconsistent with the presence of PF_6^- (or $PO_2F_2^-$) as the counterion. Moreover, the unit cell was identical with that of an authentic crystal of the BF_4^- salt, which was subsequently prepared by treatment of a CH_2Cl_2 solution of **2** with $FcBF_4$ and grown from CH_2Cl_2/ether. The origin of the BF_4^- is unknown.

Instrumentation and Procedures. (1) Electrochemical Characterization. Cyclic voltammetric, bulk electrolysis, and spectroelectrochemical experiments were carried out at (20 ± 1) °C using the same apparatus and procedures as described in ref 1. The BAS RDE-2 accessory was used for rotating disk electrode experiments. Simulations of cyclic and rotating disk electrode voltammetric experiments were performed with DigiSim (version 3.05) software.[6] One- or 3-mm-diameter glassy carbon (GC) or platinum (Pt) disks were used as working electrodes in voltammetric experiments, and a platinum gauze electrode was used in spectroelectrochemical and bulk electrolysis experiments. Potentials of all working electrodes are reported against the Fc/Fc^+ redox couple. The solutions used for voltammetric and spectroelectrochemical measurements were purged with solvent-saturated nitrogen gas prior to all experiments and blanketed with nitrogen during the course of the experiments. Electronic spectra over the wavelength range from 800 to 200 nm were recorded continuously during the course of the electrolysis at a scan rate of 504 nm min^{-1} until the electrolysis was completed.

(2) Electron Paramagnetic Resonance (EPR) Spectroscopy. EPR measurements were carried out with a Bruker ESP 380FT/CW spectrometer operating at 9.43 GHz (X band). Microwave frequencies were measured with an EIP microwave 548A frequency counter, and *g* values were determined with reference to the F^+ line in CaO (2.0001 ± 0.0002).[7] EPR spectral simulation was achieved by use of the Bruker SOPHE software package.[8]

A quartz solution flat cell (Wilmad Glass WG-808-Q) was used for the dichloromethane solution EPR studies over the temperature range of 305−185 K. Standard 3-mm-i.d. quartz tubes were employed for the frozen solution studies over the temperature range

(2) Roundhill, D. M.; Gray, H. B.; Che, C.-M. *Acc. Chem. Res.* **1989**, *22*, 55. (b) Woollins, J. D.; Kelly, P. F. *Coord. Chem. Rev.* **1985**, *65*, 115. (c) Umakoshi, K.; Sasaki, Y. *Adv. Inorg. Chem.* **1994**, *40*, 187.
(3) Kissinger, P. T.; Heineman, W. R. *Laboratory Techniques in Electroanalytical Chemistry*; Marcel Dekker: New York, 1984.
(4) Hendrickson, D. N.; Sohn, Y. S.; Gray, H. B. *Inorg. Chem.* **1971**, *10*, 1559.
(5) Brauer, G. *Handbuch der Präparativen Anorganischen Chemie;* Ferdinand Enke Verlag: Stuttgart, Germany, 1981; Vol. 3, p 1845.
(6) *DigiSim for Windows 95*, version 3.05; Bioanalytical Systems Inc.: West Lafayette, IN, 2000.
(7) Wertz, J. E.; Orton, J. W.; Auzins, P. *Discuss. Faraday Soc.* **1961**, *31*, 140.

of 110−170 K. The sample temperatures were controlled by a Bruker VT 2000 controller with a nitrogen gas flow insert fitted to the standard rectangular TE_{102} cavity. Electrochemically synthesized samples of $\mathbf{2}^+$ were prepared for EPR experiments by syringe transfer from the bulk electrolysis cell into oven-dried cells previously deoxygenated thoroughly by evacuation and filling with dry nitrogen gas. Glass spectra were obtained by freezing the dichloromethane solution of the analyte/electrolyte mixture. EPR solutions of the chemically synthesized mixed-valent platinum complex were prepared by dissolving the powder in pure dry and deoxygenated dichloromethane in the cells immediately before experiments.

(3) EHMO Calculations. EHMO (extended Hückel molecular orbital) calculations of complexes **1**, **2**, and $\mathbf{2}^+$ were undertaken using the geometry determined by X-ray crystallography (omitting solvent and anion molecules). Model calculations were also performed by replacing all of the carbon groups in the structure by H, using covalent radii to determine Pt−H and As−H bond distances, but retaining all remaining geometrical parameters from $\mathbf{2}^+$. Weighted standard parameters as implemented in HyperChem Professional Release 5.1[9] and a Hückel constant of 1.75 were employed; d orbitals were included for heavy elements as polarization functions.

(4) DFT Calculations. Density functional calculations (DFT) were performed for the structures **1**−**3** and the positively charged species $\mathbf{1}^+$ and $\mathbf{2}^+$ using Gaussian 98.[10] The Los Alamos scalar relativistic pseudopotentials, together with double-ζ valence-only basis sets for Cl, As, and Pt[11] and Dunning−Huzinaga valence double-ζ basis sets for the lighter atoms, were used.[12] Because of the large computer times involved for the geometry optimizations, we chose the local density approximation (LDA). All optimized structures are available in Cartesian coordinates as Supporting Information (Table S1).

X-ray Crystallography. Initial attempts to mount crystals of what were found to be the BF_4^- salt rather than the expected PF_6^- salt of complex $\mathbf{2}^+$ were hampered by the exceptionally high vapor pressure exerted by solvent occluded in the crystals: bubbles of solvent vapor were observed to evolve rapidly from the surface of the crystals and rise slowly through the perfluoropolyether oil in which they had been dispersed for initial examination. As this evolution slowed, the crystals were observed to crumble although still thoroughly immersed in oil. A suitable specimen was ultimately mounted by injecting a selected crystal into freshly dispensed neat Paratone oil from which it was rapidly withdrawn (in a liberal coating of the oil), affixed to a fine drawn glass capillary, transferred to the diffractometer, and flash cooled to 200 K. Diffraction images were collected[13] by means of a Nonius Kappa CCD diffractometer equipped with a 95-mm camera and graphite-monochromated Mo Kα radiation ($\lambda = 0.71073$ Å).

Reflection data were extracted and reduced by standard procedures[14,15] corrected for absorption,[16] and the structure was solved by direct methods.[17] The crystal was found to contain one complex cation, one complex anion (BF_4^-), and one well-ordered dichloromethane of solvation per asymmetric unit. Full-matrix least-squares refinement on F,[18] employing positional and anisotropic displacement parameters for all non-hydrogen atoms of a model comprising these well ordered structural components, continued to convergence. Careful examination of slant Fourier maps through the electron density in a columnar region of the structure parallel to the unit cell a axis revealed no inconsistencies with the interpretation of the occupation of this volume by highly disordered diethyl ether molecules (although the presence of charged species in this region cannot be definitively excluded). The SQUEEZE routine of PLATON[19] was applied to account for the contribution of this highly disordered region of the structure to the observed electron density, and the refinement was continued to final convergence with hydrogen atoms, included in the final model at calculated positions, riding on the atom of attachment. Pertinent crystal and refinement data are summarized in Table 1. In view of the unexpected presence of BF_4^- as the counterion in this particular crystal, a bulk sample of the BF_4^- salt of $\mathbf{2}^+$ was prepared (see Chemical Synthesis of $\mathbf{2}^+$ section) and the unit cell dimensions of crystals obtained from this synthesis were found to correspond with the values reported here.

Results and Discussion

Electrochemical Oxidation of 2. (1) Voltammetry. Qualitative details of voltammetric data obtained for the oxidation of **2** over wide potential ranges are available in ref 1. In this paper, only quantitative data related to oxidation of **2** to $\mathbf{2}^+$ are presented.

(a) Cyclic Voltammetry. Cyclic voltammograms obtained at GC and Pt electrodes in dichloromethane (0.1 M Bu_4NPF_6) over the potential range encompassing the $\mathbf{2}^{0/+}$ process exhibit a chemically and electrochemically reversible one-electron oxidation process. This is evident from the excellent agreement of experimental data and voltammograms simu-

(8) Griffin, M.; Muys, A.; Noble, C.; Wang, D.; Eldershaw, C.; Gates, K. E.; Burrage, K.; Hanson, G. R. *Mol. Phys. Rep.* **1999**, *26*, 60. Monash University is a beta-testing site for the SOPHE software described in this publication.

(9) *HyperChem*; Hypercube, Inc.: Gainesville, FL.

(10) Frisch, M. J.; Trucks, G. W.; Schlegel, H. B.; Scuseria, G. E.; Robb, M. A.; Cheeseman, J. R.; Montgomery, J. A., Jr.; Vreven, T.; Kudin, K. N.; Burant, J. C.; Millam, J. M.; Iyengar, S. S.; Tomasi, J.; Barone, V.; Mennucci, B.; Cossi, M.; Scalmani, G.; Rega, N.; Petersson, G. A.; Nakatsuji, H.; Hada, M.; Ehara, M.; Toyota, K.; Fukuda, R.; Hasegawa, J.; Ishida, M.; Nakajima, T.; Honda, Y.; Kitao, O.; Nakai, H.; Klene, M.; Li, X.; Knox, J. E.; Hratchian, H. P.; Cross, J. B.; Adamo, C.; Jaramillo, J.; Gomperts, R.; Stratmann, R. E.; Yazyev, O.; Austin, A. J.; Cammi, R.; Pomelli, C.; Ochterski, J. W.; Ayala, P. Y.; Morokuma, K.; Voth, G. A.; Salvador, P.; Dannenberg, J. J.; Zakrzewski, V. G.; Dapprich, S.; Daniels, A. D.; Strain, M. C.; Farkas, O.; Malick, D. K.; Rabuck, A. D.; Raghavachari, K.; Foresman, J. B.; Ortiz, J. V.; Cui, Q.; Baboul, A. G.; Clifford, S.; Cioslowski, J.; Stefanov, B. B.; Liu, G.; Liashenko, A.; Piskorz, P.; Komaromi, I.; Martin, R. L.; Fox, D. J.; Keith, T.; Al-Laham, M. A.; Peng, C. Y.; Nanayakkara, A.; Challacombe, M.; Gill, P. M. W.; Johnson, B.; Chen, W.; Wong, M. W.; Gonzalez, C.; Pople, J. A. *Gaussian 03*, revision B.01; Gaussian, Inc.: Pittsburgh, PA, 2003.

(11) Hay, P. J.; Wadt, W. R. *J. Chem. Phys.* **1985**, *82*, 299 and references therein.

(12) Dunning, T. H., Jr.; Hay, P. J. In *Modern Theoretical Chemistry*; Schaefer, H. F., III, Ed.; Plenum Press: New York, 1976; Vol. 3, p 1.

(13) *COLLECT*; Nonius BV: Delft, The Netherlands, 2001.

(14) Otwinowski, Z.; Minor, W. In *Methods in Enzymology*; Carter, C. W., Jr., Sweet, R. M., Eds.; Academic Press: New York, 1997; Vol. 276, p 307−326.

(15) Mackay, S.; Gilmore, C. J.; Edwards, C.; Stewart, N.; Shankland, K. *maXus Computer Program for the Solution and Refinement of Crystal Structures*; Bruker Nonius, Delft, The Netherlands; MacScience, Yokohama, Japan; and University of Glasgow, Glasgow, Scotland, 1999.

(16) Coppens, P. In *Crystallographic Computing*; Ahmed, F. R., Hall, S. R., Huber, C. P., Eds.; Munksgaard: Copenhagen, Denmark, 1970; p 255−270.

(17) Altomare, A.; Burla, M. C.; Camalli, M.; Cascarano, G. L.; Giacovazzo, C.; Guagliardi, A.; Moliterni, A. G. G.; Polidori, G.; Spagna, R. *J. Appl. Crystallogr.* **1999**, *32*, 115.

(18) Watkin, D. J.; Prout, C. K.; Carruthers, J. R.; Betteridge, P. W.; Cooper, R. I. *CRYSTALS Issue 11*; Chemical Crystallography Laboratory: Oxford, U.K., 2001.

(19) Spek, A. L. *Acta Crystallogr.* **1990**, *A46*, C34.

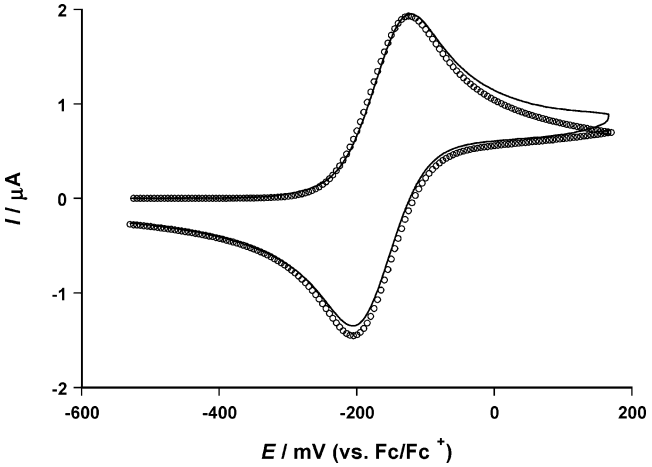

Figure 1. Comparison of experimental (—) voltammogram for oxidation of **2** and a simulated reversible voltammogram (○○○). Experimental voltammogram was obtained at 20 °C for oxidation of a 1.0 mM **2** at a 1 mm diameter GC electrode in dichloromethane (0.1 M Bu_4NPF_6) using a scan rate of 100 mV s^{-1}. Parameters used in the simulation are: $E_f^0 = -165$ mV electrode area, 0.010 cm^2; concentration, 1.0 mM; diffusion coefficient, 5.2×10^{-6} cm^2 s^{-1}; uncompensated resistance, 5200 Ω; scan rate, 100 mV s^{-1}.

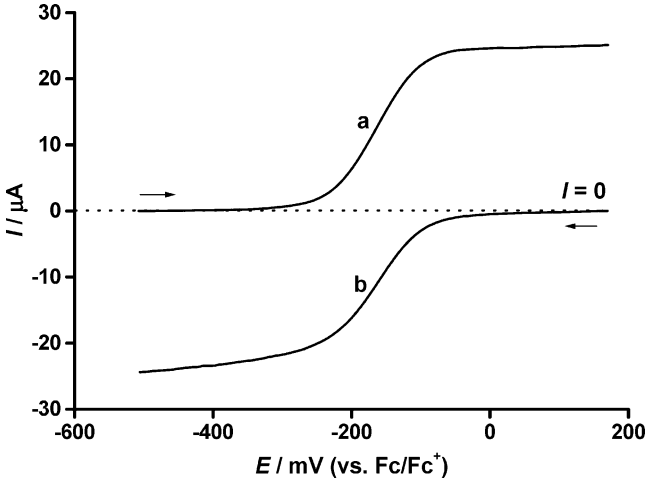

Figure 2. Voltammograms obtained at a GC rotating disk electrode (a) before and (b) after exhaustive bulk oxidative electrolysis of a 1.0 mM dichloromethane (0.1 M Bu_4NPF_6) solution of complex **2** at a potential of +170 mV (vs Fc/Fc^+). Rotation rate = 500 rpm; scan rate = 20 mV s^{-1}.

lated for a reversible one-electron oxidation process using the derived (see below) diffusion coefficient for **2** of 5.2×10^{-6} cm^2 s^{-1}, a reversible formal potential (E_f^0) of −165 mV vs Fc/Fc^+, and other parameters given in the caption to Figure 1. The fact that the average of the oxidation and reduction peak potentials [$(E_p^{ox} + E_p^{red})/2$] is constant at -165 ± 5 mV vs Fc/Fc^+ and equals the E_f^0 value obtained from the simulation over the scan rate range of 0.025−10 V s^{-1} also confirms that the process is reversible.[20]

(b) Voltammetry at Rotating Disk Electrodes. Rotating disk electrode (RDE) measurements on the oxidation process of interest were carried out at nominally 3-mm-diameter GC or Pt rotating disk electrodes. The exact electrode areas were determined to be 0.071 cm^2 for GC and 0.072 cm^2 for Pt using reduction of 1.0 mM $[Ru(NH_3)_6]^{3+}$ (diffusion coefficient of 6.2×10^{-6} cm^2 s^{-1}) in water (0.5 M KCl) and the Levich equation.[21] Comparison of experimental (Figure 2) and simulated (uncompensated resistance included) data gave a calculated reversible half-wave potential ($E_{1/2}$ value) for the $\mathbf{2}^{0/+}$ process of -165 ± 5 mV vs Fc/Fc^+. As expected, $E_{1/2} \approx E_f^0$, and the wave shape is consistent with that expected for a reversible one-electron oxidation process.

At a concentration of 1.0 mM, the limiting current was found to be linearly dependent on the square root of the angular frequencies of rotation (rotation rates of 500−3500 rpm). Conformance to the Levich relationship enabled the diffusion coefficient to be calculated as $(5.2 \pm 0.2) \times 10^{-6}$ cm^2 s^{-1} from data obtained at both GC and platinum rotating disk electrodes. All of the RDE data are fully compatible with results obtained by cyclic voltammetry.

(2) Bulk Electrolysis. During the course of oxidative electrolysis of 1.0 mM **2** at +170 mV (vs Fc/Fc^+), the dichloromethane solution changed from bright yellow to purple. RDE voltammograms obtained before and after bulk electrolysis (Figure 2) changed from a reversible one-electron oxidation (curve a) to a one-electron reduction process (curve b) and implied that almost quantitative conversion of **2** to $\mathbf{2}^+$ occurs on this time scale (tens of minutes). The current−time curve obtained during the course of electrolysis exhibited an exponential current decay, which is as expected for a straightforward $\mathbf{2}^{0/+}$ oxidation process. Coulometric analysis of these data gave an n value of 0.97 ± 0.02 electrons per molecule.

Bulk reductive electrolysis of $\mathbf{2}^+$ was carried out at a potential of −500 mV (vs Fc/Fc^+). The current−time curve again exhibited a straightforward exponential decay. The solution changed from purple back to bright yellow. Coulometric evaluation gave an n value of 0.93 ± 0.02. The RDE voltammograms recorded before and after the bulk oxidation−reduction electrolysis cycle showed a limiting oxidation current decrease of about 5% during the course of an essentially chemically and electrochemically reversible oxidation−reduction cycle of **2**. These experiments showed that $\mathbf{2}^+$ is sufficiently stable on the bulk electrolysis time scale to be amenable to chemical synthesis.

UV−Visible Spectroelectrochemical Studies. The UV−visible spectrum obtained after exhaustive oxidative electrolysis of 1.0 mM **2** differs significantly from that of **2** (Figure 3). A series of isosbestic points was observed when spectra were collected at various stages during the course of oxidation. Exhaustive reduction of $\mathbf{2}^+$ at a potential of −500 mV vs Fc/Fc^+ leads to re-formation of at least 95% of **2** (Figure 3). These data are consistent with those obtained by controlled potential bulk electrolysis and confirm that $\mathbf{2}^+$ is highly stable.

Electrochemically Informed Chemical Synthesis of $\mathbf{2}^+$. The observation that the reversible potential for the $\mathbf{2}^{0/+}$ process is more negative than that for the $Fc^{0/+}$ couple implies that reaction with Fc^+ salts should enable quantitative oxidation of **2** to $\mathbf{2}^+$ to be achieved in dichloromethane. This reaction provided the basis of the chemical synthesis of $\mathbf{2}^+$.

(20) Oldham, K. B.; Myland, J. C. *Fundamentals of Electrochemical Science*; Academic Press: San Diego, 1994; p 209.
(21) Bard, A. J.; Faulkner, L. R. *Electrochemical Methods: Fundamentals and Applications*, 2nd ed.; John Wiley & Sons: New York, 2001.

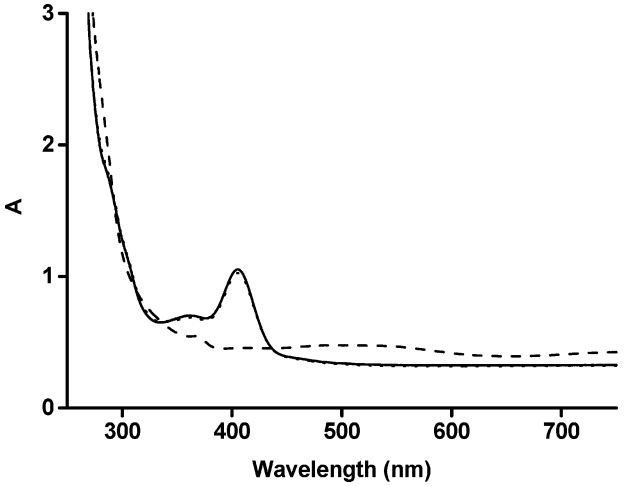

Figure 3. Electronic spectra of 1.0 mM **2** (—) before and (– – –) after exhaustive oxidative electrolysis at +170 mV and (····) after exhaustive reductive electrolysis of $\mathbf{2}^+$ at −500 mV (vs Fc/Fc^+) in dichloromethane (0.1 M Bu_4NPF_6).

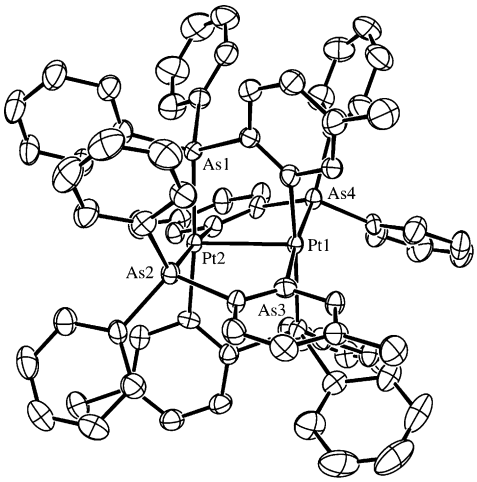

Figure 4. Molecular structure of the cation $[Pt_2(\mu\text{-}\kappa As,\kappa C\text{-}C_6H_3\text{-}5\text{-}Me\text{-}2\text{-}AsPh_2)_4]^+$ ($\mathbf{2}^+$). Hydrogen atoms have been omitted for clarity. Displacement ellipsoids are drawn at the 50% probability level.

Analysis of RDE voltammograms of **2** before and after oxidation with Fc^+ (Figure S1) confirmed that close to 100% yield could be obtained in dichloromethane.

The reaction of **2** with other one-electron oxidizing agents such as NO^+ or Ag^+ salts also generates $\mathbf{2}^+$. Single-crystal X-ray structural analysis details of the isolated solid are contained in Tables 1 and 2, and a projection of the molecular cation is shown in Figure 4.

Mixed-valent complexes with bridging halide are relatively common.[2c,22−25] However, apart from the *N*,*N*′-diarylformamidinato compound $[Pt_2(ArNCHNAr)_4]^+$ (Ar = phenyl, *p*-tolyl) reported by Cotton et al.,[26] complex $\mathbf{2}^+$ appears to be the only other lantern dinuclear mixed-valent platinum complex to be structurally characterized that is free from bridging halide ligands. Addition of halide (X^-) to $\mathbf{2}^+$ produces an equimolar mixture of **2** and **3** rather than a bridging halide complex[1] in what corresponds to the overall disproportionation reaction, given in eq 1.

$$2[Pt_2(\mu\text{-}\kappa As,\kappa C\text{-}C_6H_3\text{-}5\text{-}Me\text{-}2\text{-}AsPh_2)_4]^+ + 2X^- \rightarrow [Pt_2(\mu\text{-}\kappa As,\kappa C\text{-}C_6H_3\text{-}5\text{-}Me\text{-}2\text{-}AsPh_2)_4] + [Pt_2X_2(\mu\text{-}\kappa As,\kappa C\text{-}C_6H_3\text{-}5\text{-}Me\text{-}2\text{-}AsPh_2)_4] \quad (1)$$

This observation implies that a key factor in the successful synthesis of $\mathbf{2}^+$ is the use of a noncoordinating dichloromethane reaction environment, as addition of X_2 to **2** also produces **3**.[1]

The structure of $\mathbf{2}^+$ is similar in basic geometry to that of the parent Pt(II) complex **2**[1] and consists of four C_6H_3-5-Me-2-$AsPh_2$ groups spanning two platinum atoms, giving a

Table 1. Crystal and Refinement Data for Complex $\mathbf{2}^+$

emp formula	$C_{76}H_{64}As_4Pt_2BF_4\cdot CH_2Cl_2\cdot(C_4H_{10}O)$[a]
fw	1838.85
crystal system	triclinic
space group	$P\bar{1}$
a, Å	13.2088(1)
b, Å	14.1980(1)
c, Å	22.0121(2)
α, deg	72.3778(4)
β, deg	81.9072(4)
γ, deg	74.9263(5)
V, Å^3	3790.38(5)
Z	2
color, habit	brown, prism
cryst dimens (mm)	0.31 × 0.15 × 0.06
D_{calc} (g cm^{-1})	1.611
μ (mm^{-1})	5.54
no. indep reflns (R_{int})	17278 (0.079)
no. obsd refln [$I > 3\sigma(I)$]	9333
no. params refined	811
R	0.027
R_w	0.029
ρ_{max}/ρ_{min} (e Å^{-3})	1.14/−1.42

[a] Refer to CIF file for details.

Table 2. Selected Bond Lengths (Å) and Angles (deg) of Complexes **2** and $\mathbf{2}^+$

	2	$\mathbf{2}^+$
Pt−Pt	2.8955(4)	2.7069(3)
Pt−As	2.4064(5)	2.4432(6)
	2.4507(5)	2.4396(6)
		2.4894(6)
		2.4804(6)
Pt−C	2.071(4)	2.077(5)
	2.045(5)	2.069(5)
		2.074(5)
		2.077(5)
Pt−As−C	111.9(1)	108.2(2)
	116.2(1)	109.1(2)
		107.85(16)
		108.01(17)
Pt−Pt−As	85.359(15)	85.090(15)
	80.284(14)	87.488(15)
		86.463(15)
		85.862(15)
Pt−Pt−C	94.63(14)	94.73(15)
	100.51(14)	96.89(16)
		97.66(15)
		94.49(15)

(22) Che, C.-M.; Herbstein, F. H.; Schaefer, W. P.; Marsh, R. E.; Gray, H. B. *J. Am. Chem. Soc.* **1983**, *105*, 4604.
(23) Bellito, C.; Flamini, A.; Gastaldi, L.; Scaramuzza, L. *Inorg. Chem.* **1983**, *22*, 444.
(24) Kurmoo, M.; Clark, R. J. H. *Inorg. Chem.* **1985**, *24*, 4420.
(25) Clark, R. J. H.; Kurmoo, M.; Dawes, H. M.; Hursthouse, M. B. *Inorg. Chem.* **1986**, *25*, 409.
(26) Cotton, F. A.; Matonic, J. H.; Murillo, C. A. (a) *Inorg. Chem.* **1996**, *35*, 498; (b) *Inorg. Chim. Acta* **1997**, *264*, 61.

slightly distorted lantern-type structure, with a close-to-planar coordination geometry about each Pt atom. Similar structural features have been observed in binuclear Pt(II) and Pt(III) complexes containing P, O, N, and S donor ligands.[2b,2c,26−28] The separation of the two Pt metal centers in $\mathbf{2}^+$ of 2.7069(3) Å is considerably shorter than the separation found in **2** of 2.8955(4) Å. However, this contraction has little effect on the Pt−C bond lengths, although lengthening of ∼0.03 Å in the Pt−As distances is observed. The contraction in the Pt−Pt−C and Pt−Pt−As angles of 3−7° accommodates the closer proximity of the two platinum atoms[1] and is associated with a twist that occurs in the relative orientation of the two square-planar units upon oxidation.

Tentative assignments of the electronic spectra of complexes **2** and $\mathbf{2}^+$ can be made on the basis of literature precedent for a range of dinuclear platinum and other dinuclear metal mixed-valent complexes.[29−31] Complex **2** has a strong absorption band with a λ_{max} value of 406 nm and a broad band centered at around 362 nm, which are assigned to metal-metal-to-ligand charge transfer (MMLCT), as well as a shoulder at 290 nm, which is assigned to $\pi-\pi^*$ transitions. The chemically synthesized mixed-valent $\mathbf{2}^+$ platinum complex exhibits a UV−visible spectrum (Figure S2) similar to that of the electrochemically generated species (Figure 3), although subtle differences arising from the absence of 0.1 M Bu_4NPF_6 electrolyte are evident, which suggest that PF_6^- might associate or ion-pair with $\mathbf{2}^+$. For the chemically synthesized species, a small broad band is centered at around 1080 nm, and stronger bands with λ_{max} values of 750 nm, 534 nm (with shoulder at 490 nm), and 368 nm are evident. The absorptions at about 750 nm (ϵ = 1345 mol^{-1} L cm) and 1080 nm are likely to be due to metal-to-metal charge-transfer transitions in the mixed-valent complex. The absorption at around 368 nm and the lower energy absorption at 534 nm might be MMLCT bands.

Electron Paramagnetic Resonance (EPR) Studies. (1) Frozen-State EPR Spectra. The EPR spectrum of a 5 mM solution of chemically synthesized $\mathbf{2}^+$ in dichloromethane, frozen to 115 K, is shown in Figure 5a. Frozen dichloromethane solutions of electrochemically oxidized $\mathbf{2}^+$ gave an identical spectrum. The high-field portion of the spectrum, at higher instrumental gain, is shown as an inset. Apart from some weak resonances in the field range of 3150−3450 G, which are attributed to an impurity arising from a rearrangement or decomposition product (see below), the spectrum has the appearance expected for an axially symmetric, randomly oriented, paramagnetic dinuclear Pt complex in frozen solution, with a single unpaired electron equally distributed over the two Pt atoms. No coupling to other nuclei

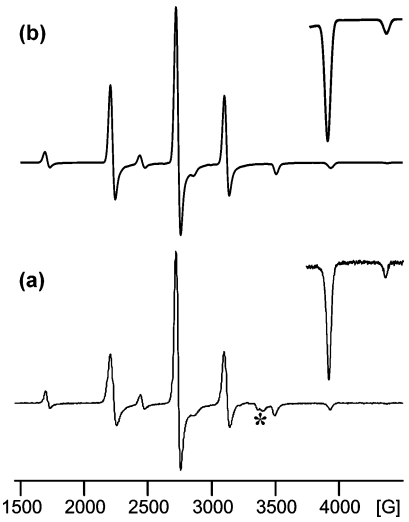

Figure 5. (a) EPR spectrum of chemically synthesized $\mathbf{2}^+$ in frozen dichloromethane solution at 115 K. Spectrometer settings: microwave power, 5.26 mW; microwave frequency, 9.418 GHz; 100-kHz modulation amplitude, 2.0 G; spectrometer gain, 2.5×10^4. Inset: High-field portion of spectrum recorded at 20 times the system gain. 100-kHz modulation amplitude, 5.0 G; spectrometer gain, 2.0×10^5. (b) Simulated spectrum of $\mathbf{2}^+$ using the parameters given in Table 4 (* rearrangement or decomposition product, see text).

(C, As) can be resolved. The main features of the spectrum shown in Figure 5a are listed, together with their origins and predicted relative intensities, in Table 3. A simulated spectrum, computed using the spin Hamiltonian parameters given in Table 4, is shown in Figure 5b. The experimental resonance field positions given in Table 3 agreed to within ±3 G with those obtained by simulations for the following three combinations of Pt isotopes: $^{195}Pt-^{195}Pt$ pairs, $^{195}Pt-^{even}Pt$ pairs, and $^{even}Pt-^{even}Pt$ pairs. It is noteworthy that the SOPHE simulation program predicted the existence of the weak feature at 4360 G prior to its observation.

The only features appearing to depend on sample preparation and subsequent treatment are those in the region from about 3150 to 3450 G (marked by an asterisk in Figure 5a). These features became more prominent after the sample was stored at −20 °C for 1 week. It is suggested that the species responsible arises from a rearrangement or decomposition product in which the unpaired electron interacts with only one Pt atom. The spin Hamiltonian parameters of this species, given in Table 4, are similar to those observed for the species formed upon partial electrolysis of $[Pt\{[(p\text{-}HC_6F_4)NCH_2]_2\}(py)_2]$ in acetonitrile.[32] The electron Zeeman *g* factors and hyperfine interactions are found to be orthorhombic.

(2) Liquid-Phase EPR Spectra. The liquid-phase spectra were examined with the expectation of being able to determine the isotropic contributions to the hyperfine tensor. However, the spectra in the temperature range from 185 K (fp $CH_2Cl_2 \approx 183$ K) to 305 K (bp $CH_2Cl_2 \approx 312$ K) exhibited features reminiscent of those reported under slow tumbling conditions for some VO^{2+} complexes.[33] Neverthe-

(27) Natile, G.; Intini, F. P.; Pacifico, C. In *Cisplatin: Chemistry and Biochemistry of a Leading Anticancer Drug*; Lippert, B., Ed.; Wiley-VCH: Weinheim, Germany, 1999; p 429.
(28) Matsumoto, K.; Ochiai, M. *Coord. Chem. Rev.* **2002**, *231*, 229.
(29) Hui, C.-K.; Chu, B. W−K.; Zhu, N.; Yam, V. W−W. *Inorg. Chem.* **2002**, *41*, 6178 and references therein.
(30) Dogan, A.; Sarkar, B.; Klein, A.; Lissner, F.; Schleid, T.; Fiedler, J.; Zâli×f0, S.; Jain, V. K.; Kaim, W. *Inorg. Chem.* **2004**, *43*, 5973 and references therein.
(31) Cotton, F. A.; Walton, R. A. *Multiple Bonds between Metal Atoms*, 2nd ed.; Clarendon Press: Oxford, U.K., 1993.
(32) Mason, D. N.; Deacon, G. B.; Yellowlees, L. J.; Bond, A. M. *J. Chem. Soc., Dalton Trans.* **2003**, 890.
(33) Campbell, R. F.; Freed, J. H. *J. Phys. Chem.* **1980**, *84*, 2668.

Table 3. Measured Field Positions and Calculated Relative Intensities of Parallel and Perpendicular Features Due to Transitions between the Energy Levels Corresponding to the Various Isotope Combinations and Nuclear Spin Wave Functions

isotope combination (I_1, I_2)	nuclear spin wave functions	parallel field position[a] (±3 G)	perpendicular field position[a] (±3 G)	relative intensity
(0, 0)	$\|0, 0\rangle$	3493	2740	15.48
($^1/_2$, 0), (0, $^1/_2$)	$\|+^1/_2, 0\rangle$, $\|0, +^1/_2\rangle$	2850	2235	7.87
	$\|-^1/_2, 0\rangle$, $\|0, -^1/_2\rangle$	3933	3120	7.87
($^1/_2$, $^1/_2$)	$\|+^1/_2, +^1/_2\rangle$	(2280)	1712	1.00
	$[\|+^1/_2, -^1/_2\rangle + \|-^1/_2, +^1/_2\rangle]/\sqrt{2}$	(3120)	2460	1.00
	$[\|+^1/_2, -^1/_2\rangle - \|-^1/_2, +^1/_2\rangle]/\sqrt{2}$	(3493)	(2740)	1.00
	$\|-^1/_2, -^1/_2\rangle$	4365	(3500)	1.00

[a] Field positions in parentheses correspond to resonances either too weak to be clearly observed in the experimental spectrum of Figure 5a or obscured by other spectral features. The components of A are taken as positive.

Table 4. Spin Hamiltonian Parameters Calculated from EPR Spectra for $\mathbf{2}^+$ and the "Rearrangement or Decomposition" Complex[a]

system	g factors			hyperfine parameters			line width
$\mathbf{2}^+$ at 115 K	$g_{\|\|} = 1.927 \pm 0.002$	$g_\perp = 2.465 \pm 0.002$		$A_{\|\|} = 940 \pm 5$	$A_\perp = 1005 \pm 5$		22 ± 5
$\mathbf{2}^+$ rapid tumbling[b]	$g_0 = 2.286 \pm 0.002$			$A_0 = 983 \pm 5$			
Rearrangement or decomposition product at 120 K	$g_x = 2.110$	$g_y = 2.010$	$g_z = 1.980$	$A_x = 65$	$A_y = 90$	$A_z = 105$	15

[a] Hyperfine parameters and line widths are in units of 10^{-4} cm^{-1}. A(Gauss) = $A(10^{-4} \times \text{cm}^{-1})/(0.46686 \times g)$. [b] Parameters calculated from frozen solution spectrum using $g_0 = (g_{\|\|} + 2g_\perp)/3$ and $A_0 = (A_{\|\|} + 2A_\perp)/3$.

less, the experimental spectrum at 305 K approached sufficiently close to that predicted for the rapid tumbling condition to justify the use of values of g_0 and A_0 calculated from the equations $g_0 = (g_{\|\|} + 2g_\perp)/3$ and $A_0 = (A_{\|\|} + 2A_\perp)/3$.

(3) Theoretical EPR Interpretation. The spectral features can be explained in terms of the spectrum expected from a combination of the isotopic mixtures (^{195}Pt−^{195}Pt, ^{195}Pt−^{even}Pt, ^{even}Pt−^{even}Pt).[34] The ^{195}Pt isotope, with nuclear spin $I = ^1/_2$, is 33.7% abundant and is the only contributor to the hyperfine splittings. The remaining 66.3% of the nuclei are even isotopes with $I = 0$. The SOPHE program performs the calculation using the three spin Hamiltonians of eq 2 and then sums the resulting spectra in accordance with the relative abundances of 4:15.48:15.48 for the nuclear spin combinations of ($^1/_2$, $^1/_2$):{(0, $^1/_2$) and ($^1/_2$, 0)}:(0, 0), respectively. The spin Hamiltonian is

$$\boldsymbol{H} = \beta[g_{\|}S_zB_z + g_\perp(S_xB_x + S_yB_y)] + \delta\sum_i [A_{\|}S_zI_{iz} + A_\perp(S_xI_{ix} + S_yI_{iy}) - \gamma\beta_n\mathbf{B}\cdot\mathbf{I}_i] \quad (2)$$

where, for ^{195}Pt−^{195}Pt, $i = 1$ and 2 and $\delta = 1$; for ^{195}Pt−^{even}Pt, $i = 1$ or 2 and $\delta = 1$; and for ^{even}Pt−^{even}Pt, $\delta = 0$ and no hyperfine structure is involved. Transition intensities are given in Table 3. All terms in eq 2 have their usual meanings, and the last term is the nuclear Zeeman interaction term where γ is the ^{195}Pt nuclear g factor and β_n the nuclear magneton. The combination of nuclear spin states when $I_1 = I_2 = ^1/_2$ gives a triplet state with $I_{total} = 1$ and a singlet with $I_{total} = 0$. The three transitions associated with the triplet hyperfine levels are shifted to lower field by second-order effects and are clearly observed, whereas the fourth, associated with the hyperfine singlet state, occurs at the same field as that of the $I_1 = I_2 = 0$ combination but is approximately only 1/16th the intensity of the latter.[34,35] In the present case, $A \approx 0.3h\nu$, and there are four transitions of equal intensity. This can be compared with the $RH_2^\bullet$ radical[35] where $A \ll h\nu$ and a 1:2:1 hyperfine pattern is observed, as a consequence of the overlap of electron spin transitions between the nuclear spin states labeled by $[|+^1/_2, -^1/_2\rangle + |-^1/_2, +^1/_2\rangle]/\sqrt{2}$ of the triplet and the singlet state labeled by $[|+^1/_2, -^1/_2\rangle - |-^1/_2, +^1/_2\rangle]/\sqrt{2}$. The impurity species in which the unpaired electron interacts with only one Pt nucleus is represented by two spin Hamiltonians, where the resonance intensities are in the ratio of the natural isotopic abundances of ^{195}Pt and ^{even}Pt.

(4) Implications of Spin Hamiltonian Parameters for Bonding. The axial symmetry of the spectrum, the magnitudes of the g values with $g_\perp > 2 > g_{\|}$, and the structure of the Pt−Pt core are consistent with the use of an analysis similar to that of Krigas and Rogers[34] on putative $[Pt_2Cl_8]^{3-}$ where the unpaired electron is in an orbital of substantially d_{z^2} character. The z direction is along the Pt−Pt axis. There is also expected to be considerable admixture of 6s character. The departure of the g values from the free-electron value, suggesting strong spin−orbit coupling to the Pt atoms; the large and almost isotropic hyperfine interaction; and the absence of any superhyperfine structure due to the As nuclei suggest that the unpaired electron is predominantly delocalized over the two Pt atoms with equal electron density on each.

The isotropic hyperfine interaction A_0, calculated from the spectral parameters of the frozen solution, is 983×10^{-4} cm^{-1}. This is large for dinuclear Pt complexes[36] and leads

(34) Krigas, T.; Rogers, M. T. *J. Chem. Phys.* **1971**, *55*, 3035.
(35) Weil, J. A.; Bolton, J. R.; Wertz, J. E. *Electron Paramagnetic Resonance: Elementary Theory and Practical Applications*; Wiley-Interscience: New York, 1994; pp 72 and 465.
(36) Klein, A.; Kaim, W.; Hornung, F. M.; Fiedler, J.; Zalis, S. *Inorg. Chim. Acta* **1997**, *264*, 269 and references therein.

to a 6s spin density of 0.086 on each Pt atom,[37] which is about double that obtained from EHMO (0.034) and DFT (0.042) calculations (see below). A second-order crystal field calculation, following Krigas and Rogers,[34] for a d_{z^2} orbital with the inclusion of covalent bonding gives a total 5d spin density of 0.965, where we have used the *g* and *A* values of Table 4 and $P = 509 \times 10^{-4}$ cm^{-1}. Again, this is rather larger than the values obtained by EHMO calculations.

Electrochemical and Chemical Oxidation of 1. The voltammetric oxidation of **1** has been suggested[1] to follow the ladder-square scheme[38−40] presented in eq 3 where **X** and $\mathbf{X}^+$ are intermediates of unknown structure. Quantitative evaluation of cyclic voltammograms combined with RDE voltammograms and EPR evidence for the postulated mechanism is now presented. The nature of cyclic voltammograms for oxidation of **1** at a glassy carbon electrode are clearly very scan rate-dependent (Figure 6a−d), but simulated voltammograms (Figure 6e−h) based on the ladder-square scheme summarized in eq 3 successfully mimic experimental data. In summary, the oxidation of **1** changed from almost fully irreversible at low scan rate (50 mV s^{-1}) to fully reversible at high scan rate (10 V s^{-1}).

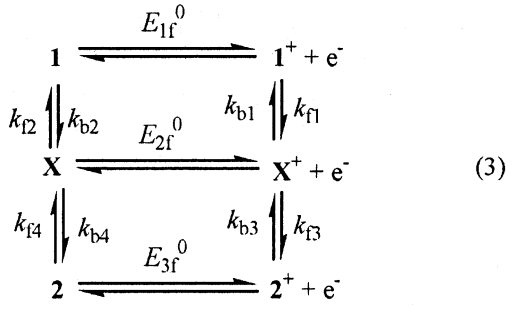

(3)

This ladder-square scheme was simulated using the DigiSim[6] software package on the basis that all three electron-transfer steps are reversible one-electron processes, the diffusion coefficients of all species are the same, and thermodynamically allowed cross redox reactions such as $\mathbf{1}^+ + \mathbf{2} \rightleftharpoons \mathbf{1} + \mathbf{2}^+$ are neglected. Unfortunately, inadequate experimental information on intermediate species **X** is available to ensure that a unique simulation is obtained in this situation where the number of unknown parameters is very large. Nevertheless, simulated voltammograms obtained with the parameters electrode area = 0.010 cm^2, concentration of **1** = 1.0 mM, diffusion coefficient for all species in reduced and oxidized forms = 5.3×10^{-6} cm^2 s^{-1}, uncompensated resistance = 6000 Ω, $E_{1f}^0 = 0.146$ V, $E_{2f}^0 = -0.0265$ V, $E_{3f}^0 = -0.170$ V, $k_{f1} = 5$ s^{-1}, $k_{b1} = 1$ s^{-1}, $k_{f2} = 10$ s^{-1}, $k_{b2} = 0.054$ s^{-1}, $k_{f3} = 5$ s^{-1}, $k_{b3} = 1.67$ s^{-1}, $k_{f4} = 2$ s^{-1}, and $k_{b4} = 0.02$ s^{-1} accurately reflect most of the key features of the experimental voltammograms shown in Figure 6a−d. However, although the three E_f^0 values and thermodynamic equilibrium constant relationships that can be derived from them are believed to be reliable, it needs to be noted that simulated voltammograms are relatively insensitive to the absolute values of some of the individual kinetic parameters. Importantly, the E_{3f}^0 value of −170 mV is very close to that expected for the $\mathbf{2}^{0/+}$ process, and the k_{f1}, k_{f2}, and k_{f3} isomerization rate constants are expected to be quantitatively significant. Thus, isomerization of $\mathbf{1}^+$ to $\mathbf{2}^+$ is clearly very much faster than the analogous **1** to **2** process.[1]

A GC rotating disk electrode voltammogram of complex **1** (Figure S3) exhibits an almost identical limiting current per unit concentration value (same rotation and scan rate employed) as found for oxidation of **2** (Figure 2). This confirms that the initial oxidation step for **1** is a one-electron process as postulated in eq 3. At a concentration of 1.0 mM, the limiting current is linearly dependent on the square root of the rotation rates (500−3500 rpm). Conformance to the Levich equation enables the diffusion coefficient of complex **1** to be calculated as $(5.3 \pm 0.2) \times 10^{-6}$ cm^2 s^{-1}. As expected, this value is very close to the $(5.2 \pm 0.2) \times 10^{-6}$ cm^2 s^{-1} value calculated for complex **2**. Similar results were obtained at a platinum rotating disk electrode.

Chemical oxidation of **1** with Fc^+ produces EPR spectra that are consistent with the formation of $\mathbf{2}^+$ and the same rearrangement or decomposition product formed as when **2** is oxidized chemically or electrochemically. However, in this case, only about 50% of $\mathbf{2}^+$ is formed on the basis of the intensity of the EPR signal. No EPR spectrum attributable to other diplatinum mixed-valent species was detected. RDE voltammograms obtained after chemical oxidation of **1** (Figure S1c) also are consistent with about a 50% yield of $\mathbf{2}^+$, as are electrochemical and spectroelectrochemical data obtained after bulk electrolysis of **1**. The side reaction responsible for the lower yield of $\mathbf{2}^+$ and increased yield of rearrangement or decomposition product in chemical and electrochemical bulk synthesis relative to yields formed when **2** is directly oxidized to $\mathbf{2}^+$ is unknown.

EHMO (Extended Hückel Molecular Orbital) Calculations. EHMO calculations were performed on **1**, **2**, and $\mathbf{2}^+$ at crystallographically determined geometries (see ref 1 for crystallographic details of **1** and **2**). In the case of **1**, the highest occupied molecular orbital (HOMO) is found at −11.71 eV. It forms part of a closely spaced band of orbitals that have Pt d character but are extensively delocalized into the ligand framework. There are six such orbitals in the energy range from −11.71 to −12.06 eV, but a clear distinction cannot be made between the Pt (d_{z^2}) orbital, normally the HOMO of a square-planar Pt(II) complex, and the other metal d orbitals. The lowest unoccupied molecular orbital (LUMO) at −8.40 eV forms part of a closely spaced band of π^* orbitals associated with the bridging and chelating phenylene groups. These π^* orbitals can act as acceptors and consequently can account for the rich electronic spectrum of complex **1** and its luminescent properties.[1]

The situation is quite different for **2**, the HOMO at −11.43 eV being well separated from a set of closely

(37) Morton, J. R.; Preston, K. F. *J. Magn. Reson.* **1978**, *30*, 577.
(38) Bond, A. M.; Keene, F. R.; Searle, N. W.; Snow, M. R. *Inorg. Chem.* **1978**, *17*, 2847.
(39) Bond, A. M.; Hambley, T. W.; Snow, M. R. *Inorg. Chem.* **1985**, *24*, 1920.
(40) Evans, D. H. *Chem. Rev.* **1990**, *90*, 739.

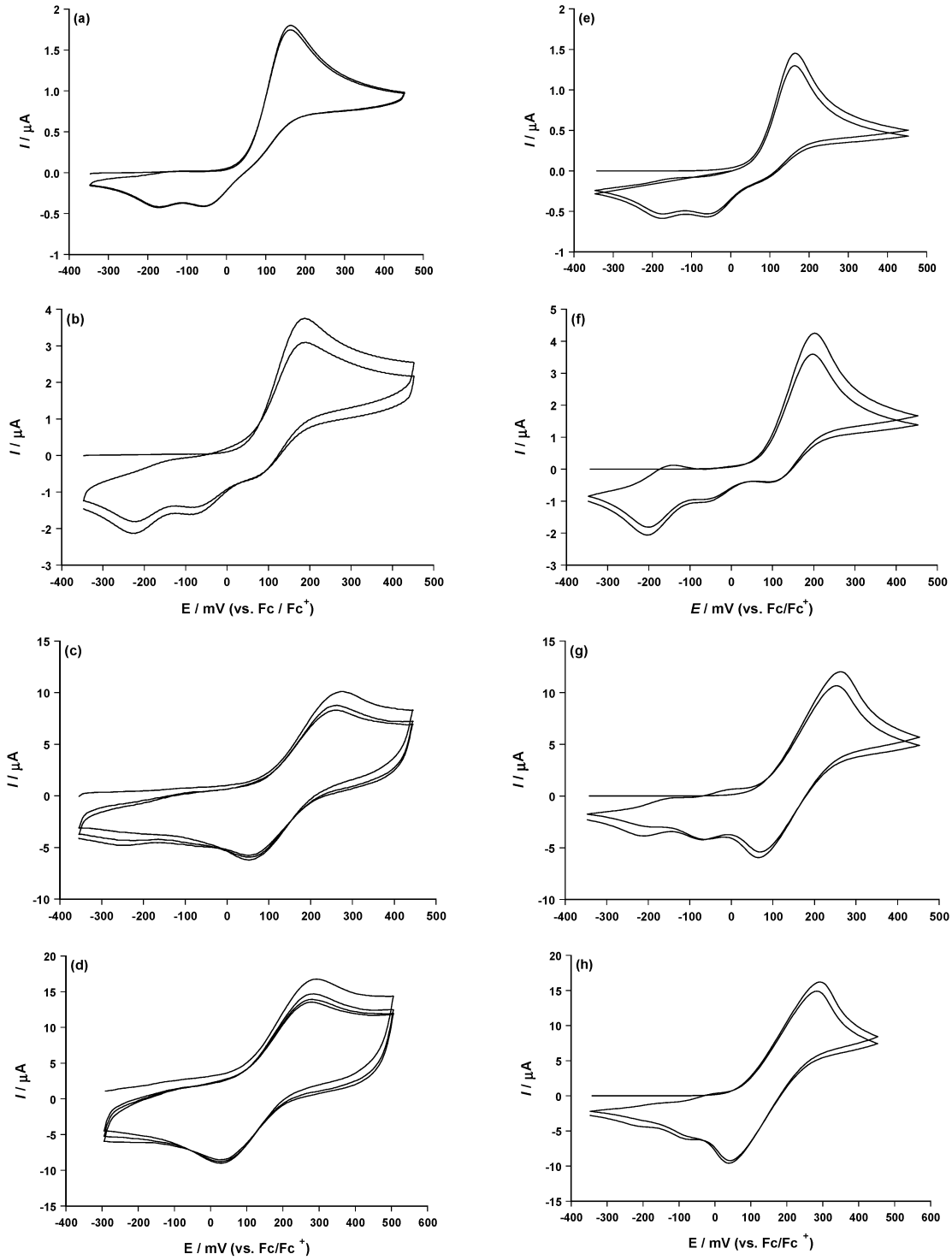

Figure 6. (a−d) Experimental and (e−h) simulated cyclic voltammograms for the oxidation of 1.0 mM complex **1** at a GC electrode in dichloromethane (0.1 M Bu_4NPF_6) at scan rates of (a,e) 50 mV s^{-1}, (b,f) 500 mV s^{-1}, (c,g) 5 V s^{-1}, and (d,h) 10 V s^{-1}. Simulation parameters are given in the text.

spaced orbitals found between −11.81 and −12.00 eV, the latter quite similar to orbitals of similar energy in **1**. The HOMO is dominated by Pt(d_{z^2})−Pt(d_{z^2}) σ*-antibonding character and is only slightly delocalized onto the bridging phenylene ligands. The LUMO is found at −8.43 eV and forms part of a band of π* orbitals of the phenyl and phenylene groups very similar to those found in **1**. The energies of the lowest electronic absorption bands of **1** (26000 cm^{-1}) and **2** (24700 cm^{-1}) also are consistent with a higher-lying HOMO for **2** but very similar LUMO energies in both complexes. This description of the electronic structure for **2** is similar to that of other Pt(II)−Pt(II) dimers that have been previously studied experimentally and computationally.[2c,31,41,42]

(41) Mealli, C.; Pichierri, F.; Randaccio, L.; Zangrando, E.; Krumm, M.; Holtenrich, D.; Lippert, B. *Inorg. Chem.* **1995**, *34*, 3418.
(42) Randaccio, L.; Zangrando, E. In In *Cisplatin: Chemistry and Biochemistry of a Leading Anticancer Drug*; Lippert, B., Ed.; Wiley-VCH: Weinheim, Germany, 1999; pp 405−428.

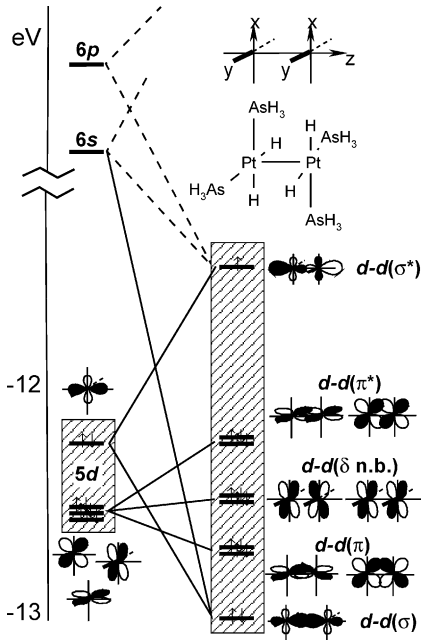

Figure 7. Orbital interaction diagram for two square-planar *cis*-$PtH_2(AsH_3)_2$ fragments (shown at left-hand side only) combining face-to-face in the geometry of $\mathbf{2}^+$. The frontier orbitals of d^8 square-planar complexes are well-known: essentially degenerate d_{xy}, d_{xz}, and d_{yz} orbitals and a higher-energy d_{z^2} orbital as the HOMO. In the dimer, mixing-in of Pt 6(s,p) character increases the bonding character of the d−d(σ) and decreases the antibonding character of the d−d(σ*) orbitals.

Removal of one electron from the Pt−Pt σ* HOMO of **2** generates the paramagnetic mixed-valent complex $\mathbf{2}^+$. The electronic structure of the cation in $\mathbf{2}^+$ closely resembles that of its precursor **2**. The singly occupied molecular orbital (SOMO) shown in Figure S4 is largely Pt(d_{z^2})−Pt(d_{z^2}) σ*-antibonding in character. Orbital mixing reduces the σ* character of the SOMO and enhances the bonding character of the corresponding Pt(d_{z^2})−Pt(d_{z^2}) σ orbital, as is clearly evident from the topology of the SOMO. The resulting mixed orbital is calculated to be 64.5% Pt(5d), 6.7% Pt(6s), and 2.5% Pt(6p), with less than 1% contribution from the ipso carbon atoms of the bridging phenylene group. This high degree of localization of the unpaired electron density on Pt is consistent with the EPR data.

Calculations were also performed on a highly simplified model complex in which all carbon groups have been replaced by hydride anions, both on Pt and on As. The bonding of this simplified cluster can be represented by the orbital interaction diagram shown in Figure 7, in which two *cis*-$PtH_2(AsH_3)_2$ square-planar platinum fragments are combined into a dimer with a Pt−Pt distance of 2.707 Å and an As−Pt−Pt−As dihedral angle of 98.9°. The d−d(π) and d−d(π*) interactions essentially cancel each other out, while the d−d(δ) interactions are nonbonding; they require a substantially shorter metal−metal distance to interact significantly. Thus the net bonding interaction involves only the d−d(σ) combination of the formal Pt(d_{z^2}) orbitals. With d−d(σ) fully, and d−d(σ*) semi-occupied, there is a formal metal−metal bond order of $^1/_2$.

DFT Calculations. The Pt−Pt separations calculated by DFT calculations at the LDA level for the symmetrical gas-phase structures are 3.063 Å (**1**), 2.732 Å ($\mathbf{1}^+$), 2.923 Å (**2**), 2.751 Å ($\mathbf{2}^+$), and 2.707 Å (**3**), which can be compared with the values for the crystalline solids already determined by X-ray diffraction of 3.421 Å (**1**), 2.896 Å (**2**), 2.707 Å ($\mathbf{2}^+$), and 2.744 Å (**3**). A limited range of trends is borne out experimentally. However, the relative ordering of the Pt−Pt distances for $\mathbf{2}^+$ and **3** is not reproduced, and agreement between the calculated and observed Pt−Pt distance for **1** is poor. These discrepancies might result from a critical dependence on environmental effects (solid vs gas) and on the level of theory applied.

The formation of **3** from **2** by oxidative addition with chlorine and the isomerizations of **1** to **2** and of $\mathbf{1}^+$ to $\mathbf{2}^+$ are all calculated to be exothermic in the gas phase, with ΔH values of −105, −12.8, and −10.5 kcal mol^{-1}, respectively, in agreement with the observations that these are thermodynamically favored processes in the solution phase.[1]

DFT data are in agreement with results of EHMO calculations in the sense that removal of one electron when **2** is oxidized to $\mathbf{2}^+$ is predicted to occur mainly at the Pt atoms to achieve 78% spin density at both Pt atoms (8.4% is s, 5.86% is p, and 63.8% is d) and 70% for $\mathbf{1}^+$. The DFT-calculated HOMO for **1** also forms part of a closely spaced band of orbitals, and the HOMO for **2** is again well separated from a set of closely spaced orbitals, although the absolute values of −7.68 eV (**2**) and −4.37 eV (**1**) differ significantly from their EHMO counterparts. Additionally, it should be noted that the theoretically predicted change in energy due to geometric relaxation in the gas phase is rather small (adiabatic ionization potentials for **1** and **2** are 5.83 and 5.93 eV, respectively) and in the reverse order to what might be anticipated on the basis of solution-phase reversible potentials. Here again, the change of environment (in this case, between solution and gas phase) and the level of theory applied can inhibit the usefulness of direct comparison between theory and experiment.

Conclusions

The cation $\mathbf{2}^+$, isolated as its BF_4^- or PF_6^- salt, represents a rare example of a structurally and spectroscopically well-characterized, dinuclear, mixed-valent platinum complex with a lantern structure. It is a persistent paramagnetic ion of considerable stability and has a characteristically symmetric EPR spectrum fully in accord with the SOMO derived by quantum mechanical calculations. The present study, in conjunction with that reported in ref 1, therefore provides a second series[26] of compounds, namely, **2**, $\mathbf{2}^+$, and **3**, with Pt−Pt bond orders of 0, $^1/_2$ and 1, respectively. In our case, in addition to crystallographic characterization of all three redox levels, the electrochemical and EPR data for the mixed-valent complex are reported.

Acknowledgment. R.T.B. thanks Prof. A. M. Bond for hosting a Sabbatical leave at Monash University that enabled him to participate in this collaborative project. Financial support from the Australian Research Council in the form of a Linkage-International award (R.T.B. and A.M.B.); from the Alexander von Humboldt Foundation, Bonn (A.H.); and

from the School of Physics and Material Engineering (J.F.B. and J.R.P.) is gratefully acknowledged.

Note Added after ASAP: This article was published ASAP on March 9, 2005, with errors in the second columns of pages 2478 and 2479. The corrected version was posted on March 11, 2005.

Supporting Information Available: X-ray crystallographic data in CIF format for complex $\mathbf{2}^{+}$, Figures S1−S4, and all optimized structures collected in Table S1 as Cartesian coordinates. This material is available free of charge via the Internet at http://pubs.acs.org.

IC048660I